Inorganic Chemistry

Article

pubs.acs.org/IC

An 18-Electron System Containing a Superheavy Element: Theoretical Studies of Sg@Au_{12}

Guo-Jin Cao,[†,§] W. H. Eugen Schwarz,*[,§,∥] and Jun Li*[,§]

[†]Key Laboratory of Chemical Biology and Molecular Engineering of the Education Ministry, Institute of Molecular Science, Shanxi University, Taiyuan 030006, China

[§]Department of Chemistry and Key Laboratory of Organic Optoelectronics and Molecular Engineering, Ministry of Education, Tsinghua University, Beijing 100084, China

[∥]Physical and Theoretical Chemistry, University of Siegen, Siegen 57068, Germany

Supporting Information

ABSTRACT: M@Au_{12} cage molecules (M = transition element from group 6) are interesting clusters with high-symmetric structure and significant stability. As the heavier homologue of W is ^{106}Sg, it is interesting to pinpoint whether the Sg@Au_{12} cluster is also stable. Geometric and electronic structures and bonding of various Sg@Au_{12} isomers were investigated with density functional theory (PW91, PBE, B3LYP) and wave function theory (MP2, CCSD(T)) approaches. The lowest-energy isomer of Sg@Au_{12} has icosahedral symmetry with significant Sg(6d)−Au(6s) covalent-metallic interaction and is comparable to the lighter homologues (M = Mo, W), with similar binding energy, although Sg follows (as a rare case) the textbook rule "*n*s below (*n* − 1)d". The 12 6s valence electrons from Au_{12} and the *six* 7s6d ones from Sg can be viewed as an 18e system below and above the interacting Au 5d band, forming *nine* delocalized multicenter bond pairs with a high stability of ∼0.8 eV of bond energy per each of the 12 Sg−Au contacts. Different prescriptions (orbital, multipole-deformation, charge-partition, and X-ray-spectroscopy based ones) assign ambiguous atomic charges to the centric and peripheral atoms; atomic core-level energy shifts correspond to some negative charge shift to the gold periphery, more so for Cr@Au_{12} than for Sg@Au_{12} or Au@Au_{12}.

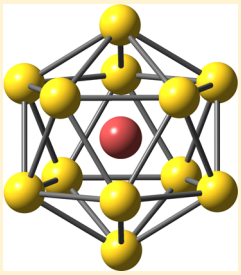

1. INTRODUCTION

Bohr had invented electronic orbits in nuclear atoms in 1913, and he derived the respective energy level patterns and maximum occupation numbers within that theoretical framework from experimental data until 1923.[1,2] Earlier, though in a purely empirical manner, Langmuir[3] had formulated atomic 8-, 18-, and 32-electron rules, which were further developed by Sidgewick, Mingos, Pyykkö, and others up to recent times.[4−6] Many examples are found in the field of transition metal complexes; see the textbooks of inorganic chemistry, for example.[7] Systems with a slightly broken spherical symmetry, such as highly symmetric transition metal complexes or atomic clusters, may have slightly broken atom-like one-particle level schemes resembling stable s^2-p^6, s^2-p^6-d^{10}, or s^2-p^6-d^{10}-f^{14} type shells for 8, 18, or 32 electrons, respectively. As Pyykkö[6] had pointed out, not all s-p-d or s-p-d-f subshells must act stabilizing or be (partially) localized on the central atom. We also note that the 18e noble gas shells of Kr and Xe are of d^{10}-s^2-p^6 type.

Pyykkö[6,8,9] had discussed the relevance of the 18e rule for metal clusters of type M′@M_n such as M′@Au_{12}, where M′ with $[(n - 1)d,ns]^6$ outer shell means an element with six valence electrons from group 6 of the periodic system, and the 12 Au atoms contribute their 12 loose outer valence electrons. The first experimental observation of icosahedral W@Au_{12} and Mo@Au_{12} clusters was reported by Wang et al.[17] in 2002 following Pyykkö's theoretical prediction earlier that year.

As usual, the atomic radii increments increase down the group (values of Fluck[10]/ Pyykkö,[11] respectively): Cr ≈ 125/122, Mo ≈ 136/138, W ≈ 137/137, and Sg ≈ 132/143 pm. The values suggested for Au show a larger discrepancy of 144/124 pm; see also refs 12 and 15. The two radii of Au resemble those of the lightest versus the heaviest group 6 elements, namely, Cr and Sg. Seaborgium is the heaviest of all elements where simple chemistry may still be possible: the $^{270\pm1}$Sg isotopes have lifetimes of ∼2 min. Various halo−oxo−hydroxo and carbonyl complex species of Sg (of even shorter-lived isotopes) in the gaseous and liquid phase have been reported as similar to Sg's lighter homologues.[13]

Concerning the effective atomic radii of Sg, the open question is whether W < Sg or W > Sg. W < Sg seems more reasonable because the Dirac−Fock radii of both the p-core and d-valence shells of Sg are 11.5% larger than those of W,[14] although Fricke advocated W ≈ Sg.[15] Sg exhibits even larger relativistic effects than those of the celebrated Au,[16] such as large 6p core and 6d valence spin−orbit splittings, 6d self-consistent relativistic expansion and destabilization, and 7s direct relativistic stabilization and contraction. The question arises, in which direction Sg@Au_{12} might deviate from well-investigated W@Au_{12}.[8,9,17,18]

Gold atoms and gold clusters have recently gained increased interest in chemistry and material science, since they can act as

Received: February 13, 2015
Published: March 23, 2015

DOI: 10.1021/acs.inorgchem.5b00356
Inorg. Chem. 2015, 54, 3695−3701

effective catalysts for a variety of important reactions.[19−24] Open-shell gold clusters with an encapsulated metal atom can be stabilized by the joint effects of shell-closing, relativity, and electron correlation (aurophilic attraction).[25,26] The geometric and electronic structures of $M@Au_{12}^{q\pm}$ clusters (M = V, Cr; Nb, Mo; Hf to Pb) have been investigated both experimentally and theoretically, applying photoelectron spectroscopy, electron scattering, density functional theory (DFT), and correlated ab initio wave function theory (WFT) approaches.[27−34] Depending on the central M in $M@Au_{12}$, icosahedral, or cuboctahedral, Jahn−Teller distorted, or floppy isomers of them were found to be more stable.[33−35]

The present article deals with the previously unexplored 18e cluster molecule $Sg@Au_{12}$. We apply DFT and various correlated ab initio approaches. Toward understanding the trends, we investigate the whole $M@Au_{12}$ series for M = Cr, Mo, W, Sg, and Au and examine the chemical bonding using various theoretical analysis formalisms. The most stable isomer of $Sg@Au_{12}$ was found to possess icosahedral I_h symmetry.

2. COMPUTIONAL DETAILS

DFT calculations were performed with the Amsterdam Density Functional program (ADF 2013.01).[35−37] The atomic core−shells were frozen (with optimized valence shells in parentheses), for Cr 1s-2p (3spd4s), Mo 1s-3d (4spd5s), W 1s-4d (4f5spd6s), Sg 1s-5d (5f6spd7s), and Au 1s-4f (5spd6s). The scalar relativistic (SR) and spin−orbit coupling (SOC) effects were taken into account by the zero order regular approximation (ZORA). Valence triple-ζ plus one polarization (TZP) and two polarization (TZ2P) basis sets of Slater type were applied.

The geometries were optimized with the generalized gradient approximations[38] of Perdew−Wang (PW91) and Perdew−Becke−Ernzerhof (PBE), converging to an energy gradient < 1×10^{-5} hartree·$Å^{-1}$ at a Kohn−Sham SCF criterion < 1×10^{-8} a.u. To compare with literature results for the lighter M atoms, single-point energy calculations were also performed using the B3LYP hybrid DFT. Vibrational frequencies were calculated to confirm that the structures are real local minima on the energy surface.

For more reliable energies, the following theoretical methods were applied in single-point calculations, using the Molpro 2012 program[39] at PBE/TZ2P geometries: HF-SCF, HF-MP2, SCS-MP2, CCSD, and CCSD(T). Relativistic SOC-averaged effective core potentials (ECP) of the Stuttgart−Cologne group were used for the cores as specified above.[40] Gaussian-type basis sets of MDF-VDZ quality[41,42] and improved CRENBS ECP basis sets from the EMSL basis-set library[43,44] were used,[41,42] where the correct primitive set for Sg is 18s19p18d15f (not 12s14p6d5f as noted on the EMSL Web site). The SOC of the $Sg@Au_{12}$ cluster was estimated by adding the energy differences from B3LYP-SR/SO-ZORA to the SR-MP2 results.

The Multiwfn 3.2.1 package of Lu and Chen[45] was applied for chemical bonding analyses. Localized molecular orbitals (MOs) were constructed with the AdNDP method of Boldyrev et al.[46] The NBO 5.0 program[47,48] was used for population analyses by the NBO method of Werinhold et al. The binding energies for $M + Au_{12} \rightarrow M@Au_{12}$ were analyzed according to the energy decomposition approach (EDA) of Ziegler, Baerends, et al.[49−51] Zero-point energies (ZPE) were taken into account throughout.

3. RESULTS AND DISCUSSION

3.1. Geometries and Stabilities. The optimized structures of several $SgAu_{12}$ isomers are displayed in Figure 1 and Table 1. The PBE/TZ2P bond lengths are ∼2 pm shorter than the ones from PW91/TZP calculations. The Sg−Au distances are near 280 pm, and the Au−Au distances are ∼280 ± 10 pm, depending on the structure. As discussed earlier, Sg appears larger than W, by ∼6 pm, while Au appears, at least in the present type of compounds, significantly larger than Cr and more similar in size to its heavier homologues, in particular Sg. The order of atomic radii, Cr < Mo ≈ W < Sg (≈ Au), follows the rule of secondary periodicity.[52]

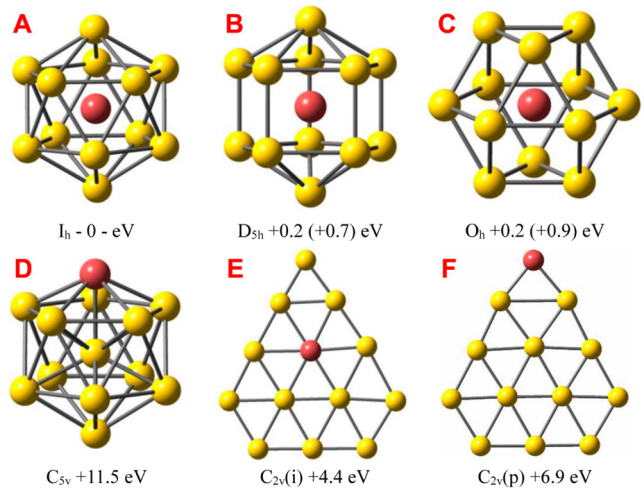

Figure 1. Optimized structures of $Sg@Au_{12}$ isomers. 3-D: (A) I_h, (B) O_h, (C) D_{5h}, (D) C_{5v}. 2-D flat: (E) C_{2v}(i), (F) C_{2v}(p) (i = Au inside, p = Au at periphery). Energies are from SR-PBE DFT, in parentheses from CCSD(T).

The relative stabilities of several $SgAu_{12}$ isomers are displayed in Figure 1 and Table 2. It shows that a larger number of Sg−Au contacts stabilizes the structure. Concerning the flat two-dimensional (2-D) Born−Oppenheimer isomers, there are various other ones with slightly different internuclear distances and slight puckering at similar or only slightly higher energies, meaning that they are all connected by vibrations, forming a soft flexible structure. Anyhow, by far the lowest-energy structures of $SgAu_{12}$ are three-dimensional (3-D) with Sg in the center. Concerning the pure Au_n clusters, they are flat for small n and 3-D for large n, the break-even point being $\sim n = 8$ for the cations and $\sim n = 12$ for the anions; the 2-D/3-D equilibrium of the neutral species occurs at $n = 11$, but the doublet species of Au_{13} has still a rather floppy structure.[53−55]

Group 6 atoms (including Sg) at the center of Au_{12} result in a closed-shell system and stabilize the 3-D symmetric structures. At the DFT level, the three 3-D $Sg@Au_{12}$ isomers are rather close in energy. At higher-quality ab initio levels, the order definitely becomes $I_h \ll D_{5h} < O_h$. The energetic order of the two lighter homologues Mo and W is $I_h < O_h < D_{5h}$ at the DFT level.[17] The preference of a low-energy O_h state is largest for Cr, namely: $O_h < I_h < D_{5h}$.[56]

The harmonic approximation of the vibrational frequencies of the I_h $M@Au_{12}$ clusters is displayed in Table 3. The totally symmetric A_g cage-breathing vibration of the centro-symmetric species is dominated by the Au−Au periphery bonding and is independent of the central mass; it varies only a little with the M−Au bond strength, namely, between 134 and 139 cm^{-1}. The first T_{1u} mode represents the motion of the central M_c atom versus the Au_{12} cage and is most dependent on the central mass and the M−Au bond strengths. The respective single M_c−Au bond force constants k_{M-Au} (in N/cm) increase from Cr (0.45) to Mo (0.65) to W (0.8) to Sg (1.0). Among the remaining 29 asymmetric Au_{12} deformation modes, only three modes (T_{2u}) increase too from Cr to Sg, while 10 modes (the two H_g) hardly vary, and 16 modes (T_{1u}, G_u, G_g, H_u) even decrease, showing the secondary periodicity Cr > Mo ≈ W > Sg.

DOI: 10.1021/acs.inorgchem.5b00356
Inorg. Chem. 2015, 54, 3695−3701

Table 1. Calculated[a] Sg−Au and Au−Au Bond Lengths R (in pm) of Optimized 3-D and 2-D Clusters of $Sg@Au_{12}$[b]

cluster			R(Sg−Au)			R(Au−Au)		
sym	state	R_p/R_c	mult	PW91 TZP	PBE TZ2P	mult	PW91 TZP	PBE TZ2P
I_h	^1A_g	1.0515	12	277.5	275.5	30	291.8	289.7
O_h	$^1A_{1g}$	1.0000	12	281.9	280.1	24	281.9	280.1
D_{5h}	$^1A_1'$	∼1.02	10	281.1	279.4	10	288.3	286.6
			2	284.3	281.6	10	285.9	283.7
						5	274.7	273.1
C_{2v}	$^1A_1$	∼1.03	6	278 ± 2	276 ± 1	14	270 ± 3	268 ± 2

[a]SR-ZORA-DFT: PW91 functional, TZP basis sets; PBE functional, TZ2P basis sets. [b]sym = symmetry of optimized structure; state = electronic ground state; mult = multiplicity of (nearly) equivalent distances; R_p/R_c = ratio of "Au−Au periphery" to "Sg−Au center" distances; the I_h ratio is symmetry-given by $\sqrt{[8/(5+\sqrt{5})]}$, and the O_h ratio is given by 1.

Table 2. Relative Energies (eV) of $Sg@Au_{12}$ with I_h, O_h, and D_{5h} Symmetries

symmetry		I_h	D_{5h}	O_h
state		^1A_g	$^1A_1'$	$^1A_{1g}$
PW91/TZP	SR	−0−	0.09	0.05
	SOC	−0−	0.11	0.06
PBE	SR	−0−	0.16	0.05
B3LYP	SR	−0−	0.01	0.05
	SOC	−0−	0.17	0.16
HF-SCF	SR	−0−	0.65	0.72
MP2	SR	−0−	0.80	1.40
	SOC[a]	−0−	0.91	1.56
SCS-MP2	SR	−0−	0.67	1.16
CCSD	SR	−0−	0.68	0.80
CCSD(T)	SR	−0−	0.67	0.87

[a]The SOC effects of the $Sg@Au_{12}$ cluster were here taken into account by adding to the MP2 results the energy differences between the SR and SOC single-point energies, as calculated with the DFT/B3LYP method.

Table 3. Vibrational Harmonic Frequencies (in cm^{-1}) of $M@Au_{12}$ (M = Cr−Sg)[a]

sym	feature	deg	Cr	Mo	W	Sg
A_g	Au_{12} breathing	1	135	136	139	139
T_{1u}	M_c vs Au_{12}	3	247	221	182	172
T_{2u}	20% increase	3	76	84	86	91
T_{1u}	15−35% decrease from Cr to Sg	3	101	81	78	67
G_u		4	103	92	94	87
G_g		4	56	50	53	48
H_u		5	43	35	36	30
H_g	nearly constant	5	116	115	118	117
H_g		5	69	71	73	71

[a]SR-ZORA-DFT/PBE/TZ2P level of theory; sym = symmetry; deg = degeneracy.

3.2. Charge Analysis. The first question about the valence electrons concerns their distribution on the cluster. Because of the large electronegativity of Au as compared to Cr, Mo, and W (and possibly Sg), the central atom of $M@Au_{12}$ is expected to be positively charged, $Q_M > 0$. However, the calculated effective charges on the atoms depend on the molecular charge density distribution as well as on the density-partitioning scheme. To explore the charge distribution we determined effective atomic charges at the DFT/PBE/TZ2P level by various prescriptions for the whole series of I_h $M@Au_{12}$ clusters (M = Cr, Mo, W, Sg, and Au, Table 4).

The effective atomic charges derived from the physically observable charge density distribution in terms of vibrating electric multipoles assign a slight electric charge transfer from well-bonded central Sg to the gold periphery, Sg → Au_{12}; that is, $Q_{Sg} > 0$, corresponding to the good Sg(6d)−Au(6s) overlap and the large electron affinity of Au. However, for the lighter M atoms at the center, less well overlapping with the Au_{12} periphery, more electrons are transferred to the center, Au_{12} → M; that is, $Q_M < 0$. For comparison, a central Au is charge-wise most similar to Sg, though already slightly negative.

Remarkably, the opposite picture is shown by orbital-based partitions, for example, by the Mulliken and Weinhold schemes, which are more and less basis set dependent. Here, more and more electrons are assigned to the central atom, the better it overlaps with the gold periphery atoms, $Q_M < 0$. A central Au atom is charge-wise now most similar to Cr. Finally, geometric or weighted partitioning schemes of the charge density according to the Hirshfeld or Voronoi-deformation prescriptions yield an intermediate picture. The charge transfers between the center and the peripheric atoms are now marginal.

Another indirect index for the effective atomic charge is the chemical shift of the atomic core-level energies, which could be obtained experimentally from X-ray photoelectron spectroscopy (XPS) and is often used to characterize the oxidation state of an element. The shifts of the Au 5s, 4f, and 5p bands of the outer Au_{12} cage of $M@Au_{12}$ are +0.18 eV for M = Cr, +0.12 eV for M = Mo, and +0.04 eV for M = W, with respect to M = Sg or Au, which have very similar cage core orbital energies. Such small shifts correspond to formal charge differences below one unit. The SOC-averaged mean band energies are Au 5s ≈ −108.3 eV, Au 4f ≈ −82.8 eV, and Au 5p ≈ −60.45 eV. The core levels of the central Au in $Au@Au_{12}$ are −1.1 eV lower, indicating a non-negligible positive charge on the central Au and some negative charge on the outer Au_{12} cage, consistent with the Voronoi and Hirshfeld density partitionings. The calculated XPS chemical shifts thus indicate an increasing positive charge on the central M atom following Au and Sg < W < Mo < Cr. It is therefore not unreasonable to consider the central atoms in these endohedral complexes existing in a positive oxidation state.

3.3. Orbital Analysis. As is well-known,[26] the relativistic effects in the valence shells of heavy atoms stabilize the s-atomic orbitals (AOs) and destabilize the d-AOs. As usual for transition metals, concerning the ionization potentials or the configuration-average orbital energies ε_{ave}, $(n-1)$d is below ns. For the heavy elements, however, the 5d < 6s gap $\Delta\varepsilon_{ave}$ is drastically reduced, for Au at the ZORA-PBE-DFT level, by

DOI: 10.1021/acs.inorgchem.5b00356
Inorg. Chem. 2015, 54, 3695−3701

Table 4. Effective Atomic Charge of Central Atom of Various I_h Symmetric M@Au_{12}[a]

			Voronoi charge			multipole derived charges		
M	Mulliken charge	Weinhold charge	ProMol	DiffDens	Hirshfeld charge	monop	dip	quadrup
Au	−0.27	−0.17	(0.05)	0.14	0.11			
Cr	−0.81	−1.60	(−0.04)	0.11	0.15	−1.12	−0.79	−0.65
Mo	−1.80	−3.25	(0.51)	0.17	0.11	−0.63	−0.62	−0.45
W	−1.79	−3.44	(0.84)	0.08	−0.02	−0.45	−0.48	−0.30
Sg	−2.67	−3.03	(1.07)	0.23	0.07	+0.37	−0.08	+0.12
Au				0.14	0.11	−0.10	−0.16	−0.05

[a]Calculations with PBE and TZ2P basis set. M is the central atom. Weinhold charge is also known as natural charge. ProMol = promolecular. DiffDens = Difference or Deformation Density. monop = monopole, dip = dipole, quadrup = quadrupole.

more than 3 eV from 4.2 eV (nonrelativistic, NR) to 1.2 eV (scalar relativistic, SR) to 0.3 eV (SOC). The relativistic effects are even larger for Sg, and they invert the common transition metal order $(n-1)$d < ns to the "textbook order" ns < $(n-1)$d. It is noteworthy that while the textbook order ns < $(n-1)$d does not really apply to any transition metal of rows 4, 5, and 6, it becomes correct due to relativity in the seventh row.[57]

A Au_{12} cluster has 60 5d AOs and 12 6s AOs, where the latter span $a_{1g} + t_{1u} + h_g + t_{2u}$ in an I_h symmetry. As there is no large orbital-energy gap above the Au $5d^{10}$ closed shells, they do not yet behave as noble-gas shells but interact with the 5d and 6s AOs of adjacent atoms. The set of Au 5d AOs forms a broad band between −9 and −6 eV at the SR-DFT-PBE level in I_h geometry (Figure 2). The Au 6s AOs interact even more

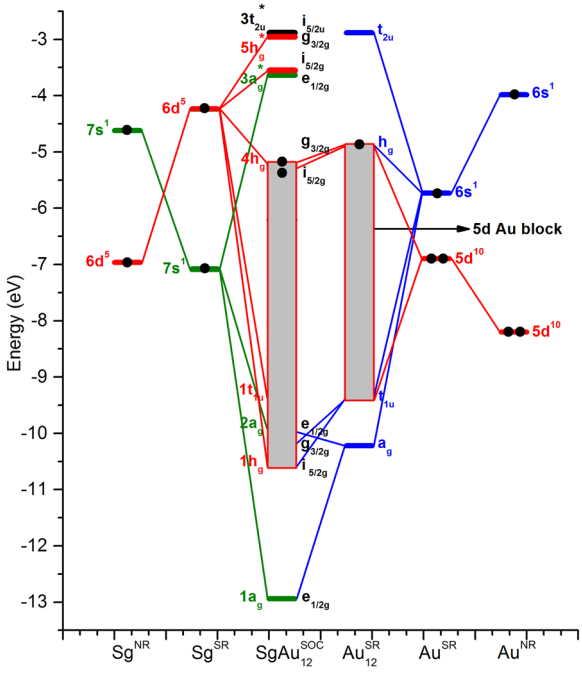

Figure 2. MO level scheme for Sg($6d^5 7s^1$), I_h Sg@Au_{12}, I_h Au_{12}, and Au($5d^{10}6s^1$), from DFT (PBE). Two dots indicate the highest closed shell; single dots indicate the highest partially occupied orbital level(s).

strongly, with MO levels below and above the Au 5d band at −10.2 eV ($1a_{1g}$),−9.3 eV ($1t_{1u}$), and at −5 eV ($4h_g$), −3 eV ($3t_{2u}$), respectively. Among the MOs of dominant Au 6s character, in particular the $1t_{1u}$ and $4h_g$ ones, are significantly mixed the $3t_{1u}$ (−6.3 eV) and $1h_g$ (−9.0 eV) levels of dominant Au5d character, causing strong Au 5d−6s hybridization. A similar situation is well-known for the d-metallic phases: the narrow lower d-band is seriously penetrated by the much broader s-band of higher average energy. We emphasize here that the concept of hybridization was introduced into quantum chemistry by Pauling in 1931, meaning the mixing of orthogonal orbitals from the *same* center (atom). We here use the word for this concept. Concerning overlapping orbital mixing from *different* centers are called covalent, dative, or coordinative interaction by the chemists. Later, solid-state and material scientists have changed the definitions of these words: In their community hybridization now indicates covalent interaction through orbital mixing from different atoms.

Concerning the Au_{12} periphery, the Au5d band is occupied by the 120 Au 5d electrons (using this classical picture only for counting the electrons), while of the 12 Au 6s electrons, eight occupy the low $1a_{1g}$ and $1t_{1u}$ MOs, and the remaining four electrons partially occupy the $4h_g$ MO. Viewed from the central point of the cluster, the angular behavior of these latter MOs is s-, p-, and d-like, as noted by Pyykkö,[6] corresponding to the common atomic orbital energy order $\varepsilon(ns) < \varepsilon(np) \ll \varepsilon(nd)$ with occupations $s^2p^6d^4$. This picture does not change much upon geometric changes (I_h deformations), except that the degenerate MOs split according to the linear Jahn−Teller effect, though with only little total energy lowering. Accordingly, the Au_{12} and Au@Au_{12} structures are rather flexible around the I_h geometry with a rather flat potential energy surface.

When an Sg ($7s/a_g$,$6d/h_g$,$7p/t_{1u}$)[6] "impurity" atom is doped into the centrally empty I_h Au_{12} cluster, it is mainly the low MOs $1a_g$ Au(s), $2a_g$ Au(d), $1t_{1u}$ Au(ds), $1h_g$ Au(sd), and the partially occupied high MO $4h_g$ Au(ds) that mix with the Sg AOs (Figure 2, Table 5). They become stabilized and fully occupied, thereby forming strong coordination bonds. These five most relevant canonical bonding MOs are shown in Figure 3.

From these analyses, the Sg−Au_{12} bonding occurs mainly through the mutual stabilization of two sets of Au_{12}(5d,6s) a_g, h_g MOs and one set of Sg(7s,6d) a_g, h_g AOs and also a little by stabilizing one set of Au_{12}(5d,6s) t_{1u} MOs by one set of virtual Sg(7p) t_{1u} AOs. In addition, the highest partially occupied h_g shell of Au_{12} is filled by electron transfer from Sg. Suppressing the Au(5d) valence participation, one may say in a simplified manner that the mixing of Sg(7s) and Au_{12}(6s) a_g yields the bonding MO $1a_g^2$ at the bottom of the valence band and the unoccupied $3a_g$* MO above, at −3.6 eV. Mixing of Sg(6d) and Au_{12}(6s) h_g yields the $4h_g^{10}$ bonding MO at the top of the valence band and the unoccupied Sg(6d) type $5h_g$* MO, at −3.2 eV, that is, above the Sg(7s) type $3a_g$* MO, corresponding to 7s < 6d of free Sg from row 7. In contrast, for the "ordinary complexes" of transition metals from rows 4, 5, 6, the empirical rule $(n-1)$d < ns applies. Eventually, the

DOI: 10.1021/acs.inorgchem.5b00356
Inorg. Chem. 2015, 54, 3695−3701

Table 5. Strongly Au−Sg Mixed Valence MOs of (I_h) Sg@Au_{12} Below and Above the Au 5d Band (see Figure 2): Symmetry, Mixing Character, Orbital Energy (in eV), Electronic Occupation Number, and AO Contributions in % (Largest is Bold)

MO	type	ε	occ	Sg(7s)	Sg(6d)	Sg(7p)	Au(5d)	Au(6s)	Au(6p)
$1a_g$	Au(s_d)+Sg(s)	−12.9	2	**44**			17	**33**	6
$2a_g$	Au(d_s)+Sg(s)	−9.4	2	8			**63**	27	2
$3a_g$*	Au(s_p)−Sg(s)	−3.6	0	17			11	**49**	23
$1t_{1u}$	Au(sd)+Sg(p)	−10.0	6			11	**40**	**42**	7
$3t_{1u}$*	Au(sp)−Sg(p)	−1.3	0			25	3	**39**	**33**
$1h_g$	Au(d)+Sg(d)	−10.4	10		25		**65**	8	2
$4h_g$	Au(ds)+Sg(d)	−5.3	10		22		**44**	22	12
$5h_g$*	Au(s_{dp})−Sg(d)	−3.2	0		**35**		11	**39**	15

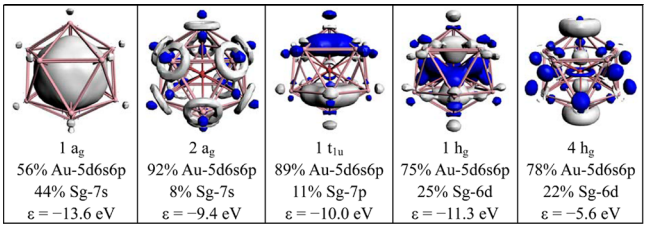

Figure 3. Contour plots of canonical Sg−Au bonding valence MOs of (I_h)Sg@Au_{12} at the DFT/PBE/TZ2P level (ψ = ±0.038 au). Note that x% Au is ∼(x/12)% for each Au.

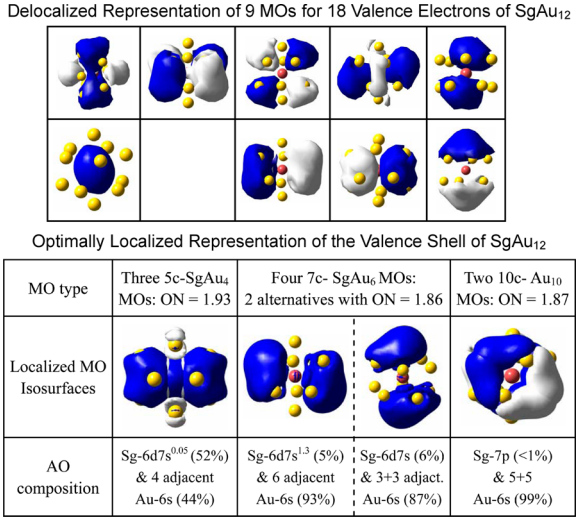

Figure 4. (I_h) Sg@Au_{12}: 9 MOs (contour values ψ = ± 0.038 au) in the Sg(7s6d)-12Au(6s) valence shell, from B3LYP/MDF-VDZ//CRENBS Adaptive Density Partitioning (AdNDP).[46] Upper part: The 18 valence electrons of $SgAu_{12}$ in doubly occupied *delocalized* MOs (Upper row: 5 "d" shaped MOs. Lower row: 1 "s" and 3 "p" shaped MOs). Lower part: 9 *optimally localized*, 5 to 10 centric MOs, one equivalent example each (ON = electronic occupation; the AO compositions are indicated).

virtual valence Sg(7p) orbitals also play some role for the bonding interactions stabilizing the Au_{12}(6s) $1t_{1u}^6$ MO. Thus, this picture resembles the 18e picture painted by Pyykkö for W@Au_{12}.[6] While the 18e noble-gas shells contain the three stable shells $(n-1)d^{10} < ns^2 < np^6$, the 18e cluster molecules contain cb-s^2 < cn-p^6 < cb-d^{10} type shells, with cb and cn meaning center-bonding and center-nearly nonbonding MOs, respectively. Further MOs without binding the central atom may be intercalated between the center-bonding cb-s^2 and cb-d^{10} type shells (Figure 2).

Using the "adaptive density partitioning" approach,[46] one can approximately extract 60 Au(5d)-type orbitals and end up with nine delocalized valence MOs of approximate "s", "p", and "d" symmetry for the remaining 18 electrons in the Sg(6d7s)−Au_{12}(6s) valence shell (Figure 4, upper). One can approximately achieve such a chemically motivated partitioning, although the envisioned 18e system is distributed over the energetic top and bottom of the valence band with the chemically active Au(5d) band being intercalated.

An alternative to the delocalized representation of the 18e system in Figure 4 (upper) is the localized representation in Figure 4 (lower). While a metallic, vanishing band gap would prevent any significant orbital localization, Sg@Au_{12} has some small though non-negligible band gap that allows for some orbital localization. However, as an electron-deficient system with only nine valence pairs for the 12 Sg−Au and 30 Au−Au contacts, the most localized MOs are at best 5 to 10 centric. As usual, they are not unique, and two alternatives for the quartets of 7c-Sg·6Au orbitals are displayed.

It has been shown[58−60] that in the T_d Au_{20} closed-shell cluster (highest occupied molecular orbital−lowest unoccupied molecular orbital (HOMO−LUMO) gap nearly 2 eV) consisting of 10 tetrahedral Au_4 building blocks, the 20 Au 6s valence electrons form 10 valence pairs, which can be represented by 10 partially localized 4c-2e bond MOs, each one in one of the 10 Au_4 units. In contrast, depending on the symmetry, the M@Au_{12} clusters are built to I_h of 20 distorted MAu_3 tetrahedra, to O_h of six distorted MAu_5 octahedra, or to D_{5h} of five $SgAu_4$ and two $SgAu_6$ building blocks. The nine valence pairs of these 18e systems do not match the topologies of the M@Au_{12} species and cannot be localized symmetrically.

3.4. Bond Energy Analysis. The binding energy ΔE_{bind} of the insertion of M = Cr, Mo, W, and Sg into the empty I_h Au_{12} cluster, M + Au_{12} → M@Au_{12}, has been investigated with the energy decomposition analysis (EDA).[49−51]

$$\Delta E_{bind} = \Delta E_{prep} + \Delta E_{elstat} + \Delta E_{Pauli} + \Delta E_{orb} \quad (1)$$

Here ΔE_{prep} is the energy cost to deform free Au_{12} to the partial structure in M@Au_{12}. ΔE_{elstat} is the classical electrostatic energy gain when the electron shells of the neutral fragments M and Au_{12} overlap. ΔE_{Pauli} is the respective quantum-mechanical overlap energy cost owing to the Pauli exclusion principle. ΔE_{orb} is the energy gain owing to orbital and occupation optimization in M@Au_{12}. The partial sum ΔE_{elstat} + ΔE_{Pauli} = ΔE_{ster} is sometimes called the steric repulsion, and the total quantum-mechanical interaction is ΔE_{Pauli} + ΔE_{orb} = ΔE_{quant}, as in eq 2. The results are listed in Table S2 of the electronic Supporting Information.

DOI: 10.1021/acs.inorgchem.5b00356
Inorg. Chem. 2015, 54, 3695−3701

$$\Delta E_{bind} = \Delta E_{prep} + \Delta E_{ster} + \Delta E_{orb} = \Delta E_{prep} + \Delta E_{elstat} + \Delta E_{quant} \quad (2)$$

Going across M = Cr, Mo, W, and Sg, all energy terms for the I_h M@Au_{12} formation increase steadily in value: the electrostatic overlap attraction ΔE_{elstat}, the quantum-mechanical overlap repulsion ΔE_{Pauli}, the steric repulsion ΔE_{ster}, the attractive quantum-mechanical molecular orbital relaxation ΔE_{orb}, and the quantum-mechanical repulsion ΔE_{quant}. However, the total insertion energies (without SOC contributions, at the B3LYP level, for I_h geometry) happen to be $-\Delta E_{bind}$ = 7.6 eV for Cr (somewhat bigger for the O_h ground state), 10.3 eV for Mo, 10.4 eV for W, 9.8 eV for Sg (and a few 0.1 eV smaller for O_h and D_{5h} metastable states). The binding energies for Mo, W, and Sg are rather similar, around 10 eV, while the binding of Cr is ~2 to 3 eV smaller due to the radially rather contracted Cr 3d orbitals.

4. CONCLUSIONS

The geometric and electronic structures of the Sg@Au_{12} cluster and its lighter homologues have been investigated with DFT (PW91, PBE) and WFT (MP2 and CCSD(T)) approaches. In contrast to Au_{12} or Au_{13} or M@Au_{12} with an M not having just six valence electrons, the presently investigated species have a closed shell and a band gap significantly above 1 eV and are geometrically less flexible. The lowest-energy isomer of the Sg@Au_{12} cluster is icosahedral as Mo@Au_{12} and W@Au_{12}. At the qualitative level, one can describe the cluster bonding by Sg(7s6d7p)−12Au(6s) orbital interaction of an 18-electron system with 12e from the 12 Au atoms and 6e from the central Sg metal atom. This picture is, however, slightly perturbed by significant Au(5d6s) hybridization and an interlacing orbital band of dominant Au_{12}(5d) character. Despite the SR and SOC reducing the HOMO−LUMO band gap of Sg@Au_{12}, the nine bonding-pair MOs can still be localized partially (at best 5 to 10 centric) over the 12 Sg−Au and the 30 Au−Au bonding contacts, though by far not as well as for Au_{20}. A remarkable point of general relevance is the energetically low position of the Sg(7s) valence orbital level, shifted due to relativity below the Sg(6d) level.

Another point of relevance is the large unphysical negative charge attached to the central heavy atom by orbital-population based concepts, that is, when applied to atoms with large (center, bulk) versus small coordination number (periphery, surface). These cage molecules thus provide a critical test set for evaluating various population analysis schemes for effective atomic charges. In consideration of the low energetic position of the Sg $7s^2$-type MO, a description of the oxidation states as $Sg^{4+}@(Au^{1/3-})_{12}$ and $M^{6+}@(Au^{1/2-})_{12}$ (M = Cr, Mo, W) seems appropriate, although oxidation state and formal charge should not be attached as an absolute physical meaning. It would be interesting to know which population analysis yields a physically relevant picture, concerning, for instance, chemical shifts of XPS or NMR signals from M of the more easily investigated M@Au_{12} species. XPS shifts are expected to indicate some loss of electron density at the centric impurity atom. While the assignments of oxidation states of central metals are not contradicting the atomic charges and bonding analysis, further experiments such as core−electron XPS are necessary to validate these conjectures.

■ ASSOCIATED CONTENT

Supporting Information

Tabulated data including energetic order of M@Au_{12} clusters of different symmetries and energy decomposition analyses for M + Au_{12} → M@Au_{12}. This material is available free of charge via the Internet at http://pubs.acs.org.

■ AUTHOR INFORMATION

Corresponding Authors

*E-mail: junli@tsinghua.edu.cn. (J.L.)
*E-mail: schwarz@chemie.uni-siegen.de. (W.H.E.S.)

Notes

The authors declare no competing financial interest.

■ ACKNOWLEDGMENTS

The calculations were supported by NKBRSF (Grant No. 2011CB932400) and NSFC (Grant Nos. 11079006 and 21433005) of China and were performed using supercomputers at Tsinghua National Laboratory for Information Science and Technology and the Supercomputing Center, Computer Network Information Center of the Chinese Academy of Sciences.

■ REFERENCES

(1) Bohr, N. *Nature Suppl.* **1923**, *2801*, 29−44.
(2) Bohr, N.; Coster, D. *Z. Phys.* **1923**, *12*, 342−374.
(3) Langmuir, I. *Science* **1921**, *54*, 59−67.
(4) Sidgwick, N.; Bailey, R. *Proc. R. Soc. London, Ser. A* **1934**, *144*, 521−537.
(5) Mingos, D. M. P. *J. Organomet. Chem.* **2004**, *689*, 4420−4436.
(6) (a) Pyykkö, P. *J. Organomet. Chem.* **2006**, *691*, 4336−4340. (b) Pyykkö, P.; Clavaguéra, C.; Dognon, J. P. In *Computational Methods in Lanthanide and Actinide Chemistry;* Dolg, M., Ed.; Wiley: New York, 2015; pp 401−424.
(7) Huheey, J. E.; Keiter, E. A.; Keiter, R. L. *Inorganic Chemistry: Principles of Structure and Reactivity;* Harper Collins: New York, 1993.
(8) Pyykkö, P.; Runeberg, N. *Angew. Chem., Int. Ed.* **2002**, *114*, 2278−2280.
(9) Pyykkö, P.; Runeberg, N. *Angew. Chem., Int. Ed.* **2002**, *41*, 2174−2176.
(10) Fluck, E.; Heumann, K. G. *The Ultimate Periodic Table;* Wiley-VCH: Weinheim, Germany, 2014.
(11) Pyykkö, P.; Atsumi, M. *Chem.—Eur. J.* **2009**, *15*, 186−197.
(12) (a) *The Chemistry of the Actinide and Transactinide Elements;* Morss, L. R., Edelstein, N. M., Fuger, J., Katz, J. J., Eds.; Springer: New York, 2011. (b) Hoffman D. C.; Lee D. M.; Pershina V. *Transactinide Elements and Future Elements;* Springer: New York, 2006; Vol. 3, pp 1652−1752. (c) Edelstein, N. M.; Fuger, J.; Katz, J. J.; Morss, L. R. *Summary and Comparison of Properties of the Actinide and Transactinide Elements,* Vol. 3, pp 1753−1835. Springer: Dordrecht, The Netherlands, 2010.
(13) Türler, A.; Pershina, V. *Chem. Rev.* **2013**, *113*,, 1237−1312.
(14) Desclaux, J. P. *At. Data Nucl. Data Tables* **1973**, *12*, 311−406.
(15) Fricke, B. *Struct. Bonding (Berlin, Ger.)* **1975**, *21*, 89−144.
(16) Pyykkö, P.; Desclaux, J. P. *Acc. Chem. Res.* **1979**, *12*, 276−281.
(17) Li, X.; Kiran, B.; Li, J.; Zhai, H. J.; Wang, L. S. *Angew. Chem., Int. Ed.* **2002**, *41*, 4786−4789.
(18) Autschbach, J.; Hess, B. A.; Johansson, M. P.; Neugebauer, J.; Patzschke, M.; Pyykko, P.; Reiher, M.; Sundholm, D. *Phys. Chem. Chem. Phys.* **2004**, *6*, 11−22.
(19) Haruta, M. *Catal. Today* **1997**, *36*, 153−166.
(20) Haruta, M.; Daté, M. *Appl. Catal., A* **2001**, *222*, 427−437.
(21) Daté, M.; Haruta, M. *J. Catal.* **2001**, *201*, 221−224.
(22) Hutchings, G. J. *Catal. Today* **2002**, *72*, 11−17.
(23) Pyykkö, P. *Angew. Chem., Int. Ed.* **2004**, *43*, 4412−4456.
(24) Wang, L.-S. *Phys. Chem. Chem. Phys.* **2010**, *12*, 8694−705.

DOI: 10.1021/acs.inorgchem.5b00356
Inorg. Chem. 2015, 54, 3695−3701

(25) Schmidbaur, H.; Schier, A. *Chem. Soc. Rev.* **2012**, *41*, 370−412.
(26) Pyykkö, P. *Chem. Rev.* **1988**, *88*, 563−594.
(27) Qiu, Y.-X.; Wang, S.-G.; Schwarz, W. H. E. *Chem. Phys. Lett.* **2004**, *397*, 374−378.
(28) Wang, S.-Y.; Yu, J.-Z.; Mizuseki, H.; Sun, Q.; Wang, C.-Y.; Kawazoe, Y. *Phys. Rev. B* **2004**, *70*, 165413.
(29) Zhai, H.-J.; Li, J.; Wang, L.-S. *J. Chem. Phys.* **2004**, *121*, 8369−8374.
(30) Graciani, J.; Oviedo, J.; Sanz, J. F. *J. Phys. Chem. B* **2006**, *110*, 11600−11603.
(31) Long, J.; Qiu, Y.-X.; Chen, X.-Y.; Wang, S.-G. *J. Phys. Chem. C* **2008**, *112*, 12646−12652.
(32) Stener, M.; Nardelli, A.; Fronzoni, G. *Chem. Phys. Lett.* **2008**, *462*, 358−364.
(33) Muñoz-Castro, A. *J. Phys. Chem. Lett.* **2013**, *4*, 3363−3366.
(34) Sato, T.; Lijnen, E.; Ceulemans, A. *J. Chem. Theory. Comput.* **2014**, *10*, 613−622.
(35) Fonseca Guerra, C.; Snijders, J.; Te Velde, G.; Baerends, E. *Theor. Chem. Acc.* **1998**, *99*, 391−403.
(36) Velde, G. T.; Bickelhaupt, F. M.; Baerends, E. J.; Fonseca Guerra, C.; van Gisbergen, S. J. A.; Snijders, J. G.; Ziegler, T. *J. Comput. Chem.* **2001**, *22*, 931−967.
(37) Baerends, E. J., et al. ADF, SCM, Theoretical Chemistry, Vrije Universiteit, Amsterdam, 2013. See http://www.scm.com.
(38) Perdew, J. P.; Burke, K.; Ernzerhof, M. *Phys. Rev. Lett.* **1996**, *77*, 3865−3868.
(39) Werner, H. J.; Knowles, P. J.; Knizia, G.; Manby, F. R.; Schütz, M.; et al. *MOLPRO*, Version 2012.1, A Package of ab Initio Programs; see http://www.molpro.net.
(40) Dolg, M.; Peterson K. A.; Schwerdtfeger P.; Stoll H., Pseudopotentials of the Stuttgart/ Cologne group, Institute for Theoretical Chemistry, University of Cologne, 2013. See http://www.tc.uni-koeln.de/PP/clickpse.en.html.
(41) Peterson, K. A.; Puzzarini, C. *Theor. Chem. Acc.* **2005**, *114*, 283−296.
(42) Figgen, D.; Rauhut, G.; Dolg, M.; Stoll, H. *Chem. Phys.* **2005**, *311*, 227−244.
(43) Schuchardt, K. L.; Didier, B. T.; Elsethagen, T.; Sun, L.; Gurumoorthi, V.; Chase, J.; Li, J.; Windus, T. L. *J. Chem. Inf. Model.* **2007**, *47*, 1045−1052.
(44) Nash, C. S.; Bursten, B. E.; Ermler, W. C. *J. Chem. Phys.* **1997**, *106*, 5133−5142.
(45) Lu, T.; Chen, F. *J. Comput. Chem.* **2012**, *33*, 580−592.
(46) Zubarev, D. Y.; Boldyrev, A. I. *Phys. Chem. Chem. Phys.* **2008**, *10*, 5207−5217.
(47) Reed, A. E.; Curtiss, L. A.; Weinhold, F. *Chem. Rev.* **1988**, *88*, 899−926.
(48) Reed, A. E.; Weinhold, F. *J. Chem. Phys.* **1983**, *78*, 4066.
(49) Ziegler, T.; Rauk, A. *Theoret. Chim. Acta* **1977**, *46*, 1−10.
(50) Bickelhaupt, F. M.; Baerends, E. J. *Kohn-Sham Density Functional Theory: Predicting and Understanding Chemistry;* Wiley-VCH: New York, 2000.
(51) Hopffgarten, M. v.; Frenking, G. *Wiley Interdiscip. Rev.: Comput. Mol. Sci.* **2012**, *2*, 43−62.
(52) Brändas, E. J., Kryachko, Eugene, S. *Fundamental World of Quantum Chemistry: A Tribute to the Memory of Per-Olov Löwdin;* Springer: Dordrecht, The Netherlands, 2004; p 659−660.
(53) Gilb, S.; Weis, P.; Furche, F.; Ahlrichs, R.; Kappes, M. M. *J. Chem. Phys.* **2002**, *116*, 4094−4101.
(54) Johansson, M. P.; Lechtken, A.; Schooss, D.; Kappes, M. M.; Furche, F. *Phys. Rev. A* **2008**, *77*, 053202.
(55) Johansson, M. P.; Warnke, I.; Le, A.; Furche, F. *J. Phys. Chem. C* **2014**, *118*, 29370−29377.
(56) Zhang, C.-H.; Cui, H.; Shen, J. *Chin. Phys. B* **2012**, *21*, 103102.
(57) House, J. E. *Inorganic Chemistry;* Elsevier: Amsterdam, The Netherlands, 2008; p 52−63.
(58) Sergeeva, A. P.; Boldyrev, A. I. *J. Cluster Sci.* **2011**, *22*, 321−329.
(59) Zubarev, D. Y.; Boldyrev, A. I. *J. Phys. Chem. A* **2009**, *113*, 866−868.
(60) King, R. B. C.; Z, F.; von Ragué Schleyer, P. *Inorg. Chem.* **2004**, *43*, 4564−4566.

DOI: 10.1021/acs.inorgchem.5b00356
Inorg. Chem. 2015, 54, 3695−3701